Probing the multi-scale interplay between gravity and turbulence – Power-law like gravitational energy spectra of the Orion Complex

Guang-Xing Li[1]⋆ , Andreas Burkert[1,2]
[1] University Observatory Munich, Scheinerstrasse 1, D-81679 München, Germany
[2] Max-Planck-Fellow, Max-Planck-Institute for Extraterrestrial Physics, Giessenbachstrasse 1, 85758 Garching, Germany

3 October 2016

arXiv:1603.05417v2 [astro-ph.SR] 30 Sep 2016

ABSTRACT

Gravity plays a determining role in the evolution of the molecular ISM. In Li & Burkert (2016), we proposed a measure called gravitational energy spectrum to quantify the importance of gravity on multiple physical scales. In this work, using a wavelet-based decomposition technique, we derive the gravitational energy spectra of the Orion A and the Orion B molecular cloud from observational data. The gravitational energy spectra exhibit power-law-like behaviours. From a few pc down to $\sim$ 0.1 pc scale, the Orion A and Orion B molecular cloud have $E_{\rm p}(k) \sim k^{-1.88}$ and $E_{\rm p}(k) \sim k^{-2.09}$, respectively. These scaling exponents are close to the scaling exponents of the kinetic energy power spectrum of compressible turbulence (where $E \sim k^{-2}$), with a near-equipartition of turbulent versus gravitational energy on multiple scales. This provides a clear evidence that gravity is able to counteract effectively against turbulent motion for these length scales. The results confirm our earlier analytical estimates. For the Orion A molecular cloud, gravity inevitably dominates over turbulence inside the cloud. Our results provide a clear observational proof that gravity is playing a determining role in the evolution these molecular clouds from the cloud scale down to $\sim$ 0.1 pc. However, turbulence is likely to dominate in clouds like California. The method is general and should be applicable to all the astrophysical problems where gravity plays a role.

Key words: General: Gravitation – ISM: structure – ISM: kinetics and dynamics – Stars: formation – Methods: data analysis

1 INTRODUCTION

Star formation takes place in the dense and shielded parts of the interstellar medium (see e.g. Dobbs et al. 2014, for a review). Magnetic fields are also believed to be playing a role (Li et al. 2014). Gravity is a long-range force, and plays a determining role in molecular cloud evolution. Observational constraints on gravity in star-forming regions are thus crucial for understanding the star formation process. However, it is not even clear if the dynamics on the cloud scale is dominated by gravity or not (Heyer et al. 2009; Kritsuk & Norman 2011). Part of the difficulty comes from the existence of complicated structures in the molecular interstellar medium (ISM) (Schneider & Elmegreen 1979; Williams et al. 2000; Goldsmith et al. 2008; Men'shchikov et al. 2010).

The virial parameter (Bertoldi & McKee 1992) is a measure of the intensity of gravity in terms of its energy measured with respect to energy from e.g. turbulent motion. To evaluate a virial parameter, one needs to define an object for which it is calculated, and is dependent on other implicit assumptions on the underlying dynamics (Ballesteros-Paredes 2006). This makes it difficult to provide constraints of gravity over multiple scales. A few attempts have been made to overcome the limitation of the virial parameter. One can evaluate the virial parameter on different physical scales by applying it to a dendrogram representation of the observational data (Goodman et al. 2009; Rosolowsky et al. 2008). Recently, Li et al. (2015) proposed a method called G-virial which generalises the concept of the gravitational potential to observations in the position-position-velocity (PPV) space. This allows one to analyse the structures of molecular gas with the G-virial maps derived from the observations. They found that molecular clouds are close to gravitationally bound when the boundaries of the regions are determined from the G-virial map. These approaches provide constraints on the importance of gravity compared to the observed turbulent motion over multiple scales. A complimentary approach is to study the *effects* of gravity. The acceleration mapping method (Li et al. 2016) is developed along this line of thought. The method computes gravitational acceleration based on maps of surface densities. It is found that gravitational acceleration behaves in a non-uniform fashion, and this can lead to fast collapse in localised regions in molecular clouds (Burkert & Hartmann 2004; Li & Burkert 2016).

What remains unconstrained is the distribution of gravitational energy across scales. This aspect is important for several theoretical reasons: first, how energy distributes across scales is a fundamental measure of a system (e.g. one fundamental way to describe

⋆ Contact e-mail: gxli@usm.lmu.de

© 2015 The Authors

the electromagnetic wave is to construct is spectrum). A second motivation is that supersonic turbulence is believed to be important in the dynamics of molecular clouds (Mac Low & Klessen 2004). The distribution of kinetic energy of the turbulent motion can be derived theoretically, and it obeys roughly $E \sim k^{-2}$ where k is the wavenumber. One can study the interplay between turbulence and gravity over multiple scales, provided that a similar measure of gravitational energy can be obtained.

Along this line of thought, Li & Burkert (2016) proposed a formalism to represent the multi-scaled structure of the interstellar medium (ISM) gravitational field and to quantify its impact on cloud evolution by constructing a quantity called *gravitational energy spectrum*. The derived gravitational energy spectra are directly comparable to e.g. the turbulence power spectra. By studying the gravitational energy spectra of a sample of 8 molecular clouds, Li & Burkert (2016) found that molecular clouds are close to a state where the kinetic energy of turbulence and gravitational energy reaches a near equi-partition. For star-forming clouds, gravity gradually takes over turbulence as one moves from larger to smaller scales.

The fact that the gravitational energy can balance and even dominate over turbulent motion in star-forming clouds has important implications in cloud evolution theory. It provides support for cloud evolution models such as the hierarchical gravitational collapse model (Hoyle 1953; Elmegreen 1993; Vázquez-Semadeni et al. 2003). See also Burkert & Hartmann (2013). These theoretical possibilities should be further explored. However, in Li & Burkert (2016), the results are inferred from the surface density PDF, where a shell model was assumed. Although the authors provided justifications why these assumptions are valid, a more detailed study is desired to validate the simplications made in their model.

We provide observational constraints on the importance of gravity by combining: (a) state-of-the-art observations of the surface density structure of molecular clouds constructed from ESA's Planck and Herschel observations (Lombardi et al. 2014), (b) constructing 3D volume density distributions from observational data, the method we use is an improved version of the method described in Kainulainen, Federrath & Henning (2014), (c) a formalism to quantify the importance of gravity on a multiple of scales, proposed in Li & Burkert (2016) and (d) a wavelet-based technique to decompose the gravitational field into multiple components.

We study the gravitational energy spectra of the clouds in the Orion molecular cloud complex. The cloud is the most massive active star-forming complex in the solar neighbourhood (Bally 2008), and is subject to intensive studies. Based on the slope of the surface density PDFs derived in Lombardi et al. (2014), Li & Burkert (2016) obtained constraints on the gravitational energy spectra for both the Orion A and the Orion B molecular cloud. They conclude that Orion A molecular cloud is in a stage where gravity takes over turbulence on smaller scales, and for Orion B they found that the cloud is close to a critical state where the gravitational energy and turbulence kinetic energy reaches equi-partition.

In this paper, we propose a wavelet-based method to construct multi-scale gravitational energy spectra from observational data. The method is general, and can be applied to structures with arbitrary geometries. In Sec. 2 we introduce the concept of the gravitational energy spectrum. We reconstruct the 3D density structure of the Orion molecular clouds from the observational data (Sec. 3). Gravitational potentials of the clouds are constructed based on the 3D density structures (Sec. 4). A wavelet-based decomposition technique is used to obtain constraints on gravity over a multitude of physical scales (Sec. 5). The results are presented in Sec. 6. In Sec. 7 we compare the observed gravitational energy spectra with the gravitational energy spectra of a Mach 5.6 compressible turbulence. This also allows us to access the performance of our method under a situation where the underlying geometry is sufficiently complicated. In Sec. 8 we compare our method with other pre-existing methods. In Sec. 9 we conclude.

2 PROBING CLOUD FRAGMENTATION WITH GRAVITATIONAL ENERGY SPECTRA

The meaning of the gravitational energy spectrum is illustrated in Fig. 1. In astrophysical settings, a density distribution $\rho(x, y, z)$ is composed of structures of different sizes. Smaller structures tend to have higher densities, and tend to reside inside larger structures. On the coarsest (largest) scale, one can measure the masses m_0 and sizes l_0 (which satisfy $l_0^{\rm min} < l_0 < l_0^{\rm max}$ where $l_0^{\rm min}$ and $l_0^{\rm max}$ are the lower and upper bounds of the scale l_0) of the structures, and the gravitational energy of the cloud on the coarsest scale is $\mathcal{E}_{l_0} = Gm_{l_0}^2/l_0$. On a smaller scale, the cloud is composed of subregions of sizes $l_1^{\rm min} < l_1 < l_1^{\rm max}$ and masses $m_{l_1(i)}$, and the total gravitational energy on this scale is $\mathcal{E}_{l_1} = \sum_i Gm_{l_1(i)}^2/l_1$. One can further increase the resolution, and compute the gravitational energy on even smaller scales e.g. $l_2, \ldots l_n$ until the resolution limit of the data has been reached. By investigating the dependence of E_l on l one can obtain a multi-scale picture of gravitation energy in molecular clouds. For a cloud that has a simple morphology, this can be achieved analytically (Li et al. 2016). Note that the picture here is proposed to help achieving an intuitive understanding of the gravitational energy spectrum. An equivalent yet mathematically rigours way to define the gravitationally energy spectrum can be achieved by decomposing the gravitational potential ϕ into components of different scales ϕ_l and evaluate $\int \rho\phi_l {\rm d}^3x$. This is described in Sec. 5.

To achieve mathematical consistency, one also needs to normalise the gravitational energy $\mathcal{E}$ by the range of physical scales within which $\mathcal{E}$ is calculated. Either one has to work with $E_l = \mathcal{E}/(l^{\rm max} - l^{\rm min})$ or with $E_k = \mathcal{E}/(k^{\rm max} - k^{\rm min})$ where $k = 2\pi/l$, l is the scale and k is the wavenumber. The gravitational energy spectra presented in this paper are normalized according to k. Therefore E_k has a unit of energy divided by wave number [1].

The gravitational energy spectrum defined in this work is a generalisation of those discussed in Li & Burkert (2016). The improvement is the regions are now allowed to have arbitrarily complicated geometries, and in Li & Burkert (2016) only close-to-spherical geometries are considered.

3 OBSERVATIONS AND SURFACE DENSITY MODELLING

We obtain observational data from Lombardi et al. (2014). The map traces column densities $1 \times 10^{21}{\rm cm}^{-2} < N < 2 \times 10^{23}{\rm cm}^{-2}$, and resolve down to $\sim 36''$ (correspond to 0.07 pc at a distance of 414 pc (Menten et al. 2007)).

Kainulainen, Federrath & Henning (2014) developed a technique to construct 3D density distributions from observational data. The idea is based on a simple assumption that a smaller gas clump observed in 2D is related to a smaller clump in real 3D space. Thus,

[1] Depending on the situation, one can also choose to further normalise it by the mass m.

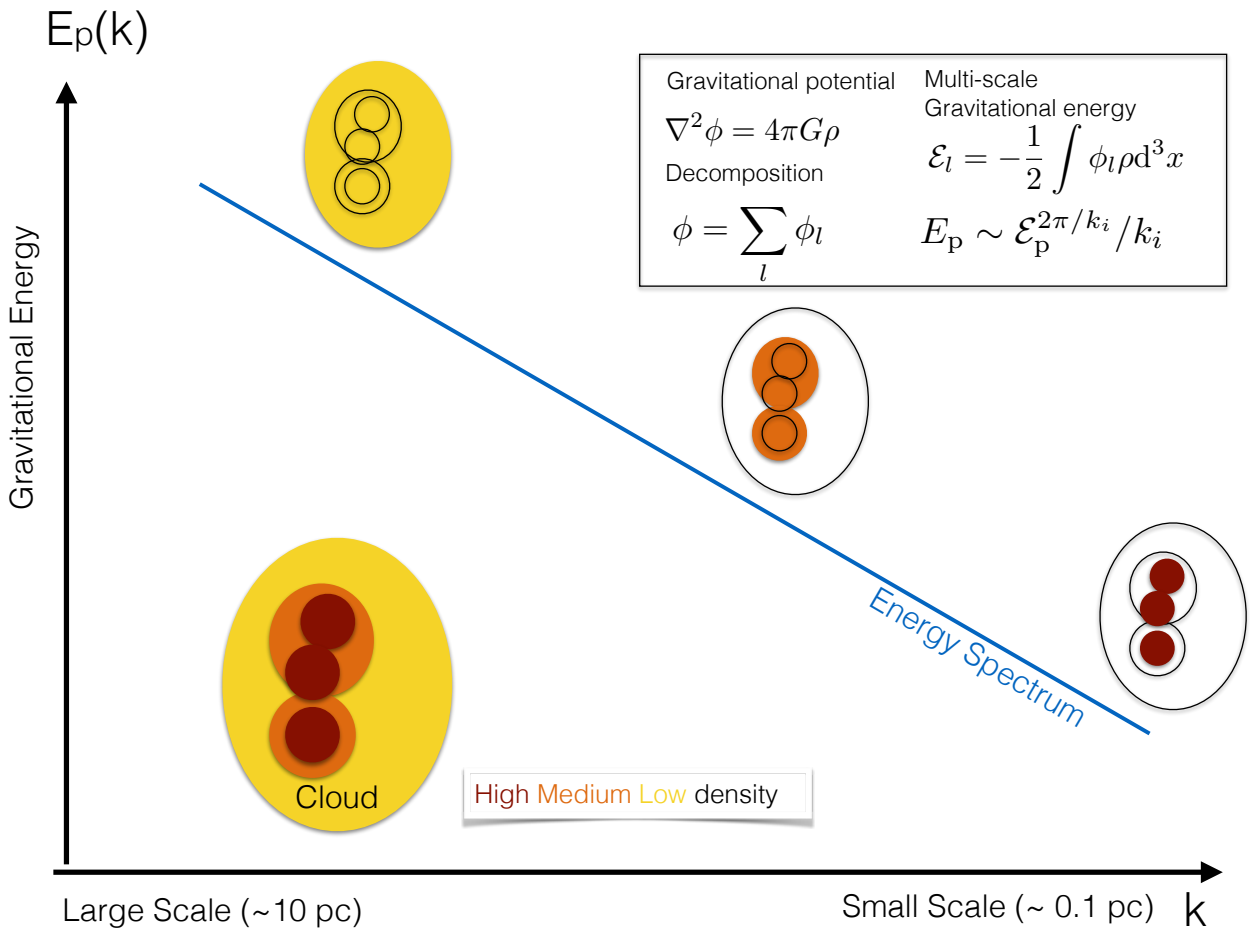

Figure 1. An illustration of the concept of the gravitational energy spectrum. In an idealised picture, one can view an object as being composed of a set of nested structures. Smaller structures (in red) tend to have higher densities, and tend to reside in larger structures (in orange and yellow). In our gravitational energy spectra plot, the x-axis is the wave number $k = 2\pi/l$, which is inversely proportional to the length scale l. The y-axis is the gravitational energy density (which has a unit of energy divided by the wave number k). Gravitational energy on the large scale is usually contributed from structures of larger sizes (in yellow), and gravitational energy on small scales is contributed from structures of small sizes (in red). See Sec. 2 for explanations. The detailed mathematical formula for evaluating the gravitational energy spectra are listed in the box. The formulas are presented and explained in Sec. 5.

the density structure of a molecular cloud can be reconstructed by decomposing the observational map into a set of 2D ellipses and by linking the ellipses to 3D ellipsoids.

Kainulainen, Federrath & Henning (2014) took a two-step approach to reconstruct 3D density distributions. First, a 2D projected observational map is decomposed into components of different sizes, generating a so-called size map. Second, each size map is decomposed into a set of structures with masses M_i and areas A_i. The extent H_i of each of the structure in the third dimension is estimated. An ellipsoid in 3D can be reconstructed based on M_i, A_i and H_i for each structure.

In this work, we reconstruct 3D density distributions using a method that shares a similar spirit with that of Kainulainen, Federrath & Henning (2014). However, several critical improvements have been made. First, we have developed an improved method to decompose the map into contributions from structures of different sizes, generating the "size map". Kainulainen, Federrath & Henning (2014) used a wavelet-based method to construct the size map. However, for the Herschel-Planck surface density map used in this work, because of the improved dynamical range, the wavelet-based method produces negative artefacts around regions where the column densities have been significantly enhanced. We thus developed an improved decomposition method where significant structures of different scales are identified by an iterative approach. The size map derived from our improved method is completely free of negative artefacts. Details of the improved method can be found in Appendix A.

In the second step, structures are identified from the size map. Properties such as masses and sizes are evaluated. This information is then used to construct a 3D volume density map. Kainulainen, Federrath & Henning (2014) used the algorithm "clumpfind" (Williams et al. 1994) to detect structures. Masses and sizes of these structures are estimated. By assuming that they are 3D ellipsoids, a 3D volume density map can be reconstructed. In the formalism of Kainulainen, Federrath & Henning (2014), the ellipsoids have sharp boundaries. These artificial boundaries do

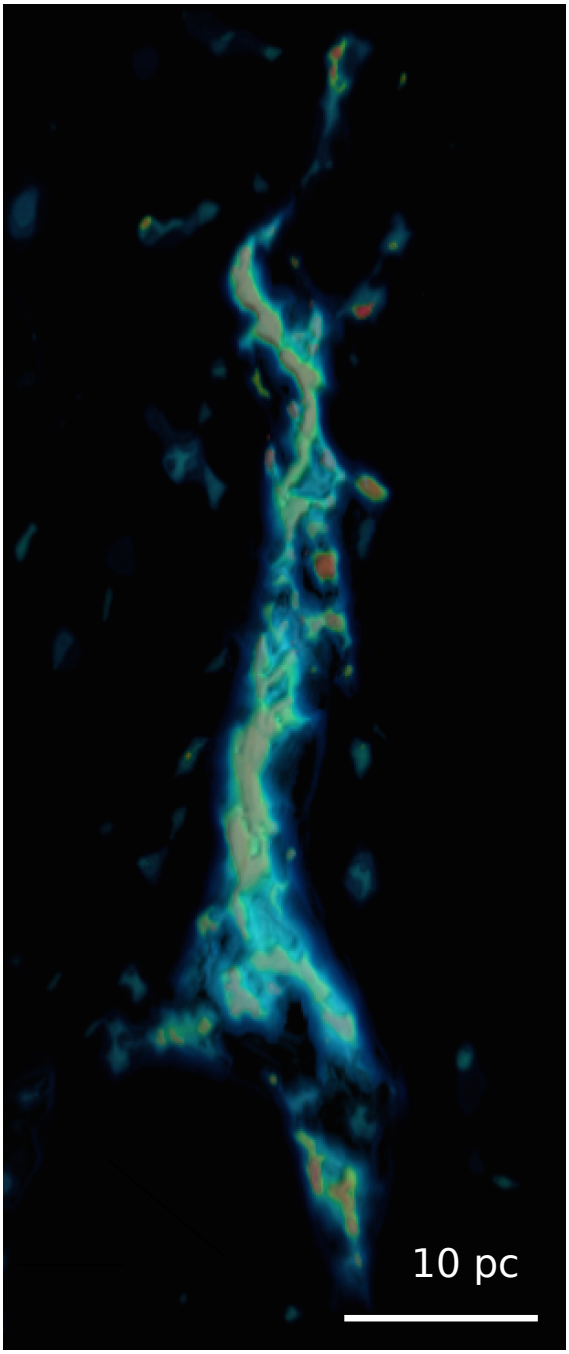

Figure 2. A 3D volume rendering of the reconstructed volume density structure of the Orion A molecular cloud. The rendering is sensitive to gas with $n_{\rm H_2} \sim 2 \times 10^4$ cm^{-3}. Filamentary structures are preserved in our new reconstruction. A scalebar is included in the plot.

not affect the volume density PDF, but are not desirable for other applications. To overcome this difficulty, we have implemented a contour-based algorithm called contour-decompose to reduce the artefacts produced at the boundaries of the ellipsoids. The details of the algorithm can be found in Appendix B. The improved algorithm produces new data sets that are better for general-purpose analysis. In Fig. 2 we present a volume rendering of the reconstructed 3D volume density map of the Orion A molecular cloud. Filamentary structures are preserved in our new reconstruction.

4 COMPUTATION OF THE GRAVITATIONAL FIELD

The gravitational potential is computed by solving the Poisson Equation $\nabla^2\phi = 4\pi G\rho$. It can be solved efficiently in the Fourier space according to

$$\phi_k = \frac{-4\pi G}{k^2}\rho_k \ , \tag{1}$$

where ϕ_k and ρ_k are the Fourier transforms of $\phi(x, y, z)$ and $\rho(x, y, z)$ respectively.

Computing gravitational potentials in the Fourier space automatically assumes that the boundary conditions are periodic. To minimise the effects of this limitation to our results, zero density paddings are added to the 3D volume density map before the computation. Note also that molecular clouds are never isolated but part of an inter-connected network of molecular structures that might affect the clouds gravitationally. This would have an effect on the gravitational energy spectrum at scales larger than e.g. half the box size. The volume density map after the padding procedure has a size of (N, N, N) where N is the maximum of the lengths of the 3 axes of the input data.

5 DERIVING THE GRAVITATIONAL ENERGY SPECTRA

We evaluate the gravitational energy spectra from observational data based on the reconstructed 3D volume density map $\rho(x, y, z)$ and the gravitational potential $\phi(x, y, z)$.

We employ a two-step approach. First, we use the wavelet transform *a trous* (see e.g. Starck et al. 1998) to decompose the gravitational potential ϕ into components of different physical scales ϕ_l (where l denotes the characteristic length scale of a particular wavelet component):

$$\phi(x, y, z) = \sum_l \phi_l(x, y, z) + R(x, y, z) \ , \tag{2}$$

where l represents the physical scale. $l_i = 2^i \, {\rm d}x$ where $i = 0, 1, 2, \ldots, n$, and ${\rm d}x$ is the map resolution. $R(x, y, z)$ is the residual. [2]. The different components are obtained by taking the Fourier modes at different intervals of spatial frequencies, and the wavelet component at scale l is contributed from Fourier modes whose scales are limited between $l/\sqrt{2}$ and $\sqrt{2}\,l$. Because long, filamentary structures have plenty of fluctuations on scales comparable to their widths, in the formalism of the wavelet transform, they can appear on scales that are comparable to their widths.

For each 3D gravitational potential map of size $(N_{\rm x}, N_{\rm y}, N_{\rm z})$, we added zero paddings around the map so that a new map is created with a size (N, N, N) where $N = \max(N_{\rm x}, N_{\rm y}, N_{\rm z})$ is created. The minimum physical scale is limited by the map resolution. Because we do not have information of structures of gas beyond the observed map, the maximum physical scale is determined by $l = 2^n {\rm d}x < \min(N_{\rm x}, N_{\rm y}, N_{\rm z})/2 \times {\rm d}x$.

Since $l_i = 2^i {\rm d}x$ where $i = 0, 1, 2, \ldots, n$, for a given l_i, $E^l_{\rm p}$ represents the gravitational energy distributed between $l_{\rm min} = l_i/\sqrt{2}$ and $l_{\rm max} = l_i \times \sqrt{2}$.

The gravitational binding energy $\mathcal{E}^l_{\rm i}$ of the wavelet component of length l is

$$\mathcal{E}^l_{\rm p} = -\frac{1}{2}\int \rho \ \phi_l \ {\rm d}x{\rm d}y{\rm d}z \ , \tag{3}$$

[2] We use the Mexican hat wavelet, https://en.wikipedia.org/wiki/Mexican_hat_wavelet.

which ensures that $E_{\rm p}^{\rm tot} = \sum_l \mathcal{E}_{\rm p}^l$ where $E_{\rm p}^{\rm tot}$ is the total gravitational binding energy of the cloud.

The gravitational energy per given length is defined as

$$E_{\rm p}^{l\rightarrow l_i} = \frac{\mathcal{E}_{\rm p}^l}{l_{\rm max} - l_{\rm min}} = \frac{\mathcal{E}_{\rm p}^{l_i}}{(\sqrt{2} - \sqrt{2}^{-1}) \times l_i} \approx \frac{\mathcal{E}_{\rm p}^{l_i}}{0.7 \times l_i} \tag{4}$$

It is more convenient to convert Eq. 4 into $E_{\rm p}(k)$ where k is the wavenumber ($k_i = 2\pi/l_i$):

$$\begin{aligned} E_{\rm p}^{k\rightarrow k_i} &= E_{\rm p}^{l\rightarrow 2\pi/k_i} \frac{2\pi}{k_i^2} \\ &\approx 1.4 \times \frac{\mathcal{E}_{\rm p}^{l\rightarrow 2\pi/k_i}}{k_i} , \end{aligned} \tag{5}$$

where we have used $|{\rm d}l/{\rm d}k| = 2\pi/k^2$, and $E_{\rm p}^l$ was defined in Eq. 4. Following Li & Burkert (2016), we call $E_{\rm p}(k)$ the *gravitational energy spectrum* of a cloud.

$E_{\rm p}(k)$ contains information on how the gravitational energy of a molecular cloud is distributed among different physical scales. Its unit is the same as that of the turbulence power spectrum. By comparing $E_{\rm p}(k)$ with the turbulence power spectrum one can evaluate the relative importance of turbulence and gravity on different physical scales.

6 RESULTS

Lombardi et al. (2014) found that the Orion A and Orion B molecular clouds have different scaling exponents of the surface density PDFs, implying that they are probably at different evolutionary stages. In this work, we treat them as different objects, and study their gravitational energy spectra separately.

The gravitational binding energy of a wavelet component of length l is defined in Eq. 2, and a visualisation of $\phi_l(x, y, z)$ provides information concerning the spatial distribution of the gravitational binding energy that belongs to component l. In Fig. 3 we present visualisations of a few wavelet components of the gravitational potential of the Orion A molecular cloud. When l is small, the gravitational binding energy comes from highly filamentary, thin gas structures in the cloud; and when l is large, the gravitational binding energy is contributed from a smoother distribution.

The gravitational energy spectra of the Orion A and Orion B molecular clouds are presented in Figs. 4, 5, respectively. For both clouds, the gravitational energy spectra exhibit power law forms. The scaling exponents are close to 2. We fitted power laws to these gravitational energy spectra by taking all the measurements with $l \lesssim$ 1pc. For Orion A we find $E_{\rm p}(k) \sim k^{-1.88}$ and for Orion B $E_{\rm p}(k) \sim k^{-2.09}$. A stepper slope means energy decreases faster with decreasing length scales. Thus, on average, the Orion A molecular cloud has more gravitational energy per unit wavenumber on smaller scales as compared to Orion B.

On the largest scale, molecular clouds are close to being gravitational bound (Roman-Duval et al. 2010; Heyer et al. 2009), and the amount of turbulent energy is comparable to the gravitational binding energy. Many of the star cluster-forming clumps in the clouds are also in apparent virial equilibrium (Wienen et al. 2012). Li et al. (2015) have demonstrated that by carefully choosing the boundaries of the regions and applying the standard virial analysis, the cloud is much more gravitationally bound compared to the result from a direct virial analysis for the while cloud. A direct connection between gravity and observed turbulent motion can also be seen from the $\alpha_k - \alpha_G$ plot (Traficante et al. 2015). Accretion has been considered as a primary source that drives turbulence in the cloud (Klessen & Hennebelle 2010). It this is the case, then one does not expect clouds to deviate from the virial equilibrium by much. Recent simulations also indicate that gravitational collapse is enough to explain the observed level of turbulent motion (Ibáñez-Mejía et al. 2015). Thus, we assume that gas is gravitational bound on the cloud scale.

The scaling exponent of the gravitational energy spectra can be compared with the kinetic energy spectra of the Burgers turbulence. For Kolmogorov turbulence $E_{\rm turb}(k) \sim k^{-5/3}$ and for Burgers turbulence $E_{\rm turb}(k) \sim k^{-2}$. The turbulence in molecular cloud is believed to be closer to Burgers (Federrath, Klessen & Schmidt 2008). Here, for both clouds, the scaling exponents of the gravitational energy spectra are indeed close to the turbulent kinematic energy spectra. To first order, this implies a multi-scale equi-partition of turbulent and gravitational energy. Thus, if on the large scale, turbulence and gravity can reach rough equilibrium, then on any smaller scales gravitational energy is least comparable to the energy from the turbulent cascade. For the Orion A molecular cloud, the gravitational energy spectrum is shallower than Burgers. At sub-parsec scale the gravitational energy should should therefore become more important than turbulence, and dominate the cloud evolution.

Li & Burkert (2016) gave an analytical expression, allowing one to infer the gravitational energy spectrum from the observed surface density PDF of the clouds. Based on observations of Lombardi et al. (2015), they derived the scaling exponents of the gravitational energy spectra for both clouds. Here, we compare the gravitational energy spectra derived using our wavelet-based analysis with those derived using the observational-analytical approach in Li & Burkert (2016). The results are summarised in Table 1. The scaling exponents derived from observations are in excellent agreements with those derived from the surface density PDFs using the analytical formula, to an accuracy of $\lesssim$ 10 %, suggesting that the formalism developed in Li & Burkert (2016) does capture the essential features of the cloud that are necessary for proper evaluations of $E_{\rm p}(k)$.

The gravitational energy spectrum is a flexibly measure. In this work, we only demonstrated the computation of gravitational energy spectra for clouds like Orion A and Orion B. In practise, it is also possible to evaluate the gravitational energy spectra for individual sub-regions in the cloud. This can be achieved by changing the integration range in Eq. 3 . This would enable us to investigate the spatial variations of gravitational energy spectra within a given cloud (similar the investigation of column density PDF evolution in Stutz & Kainulainen (2015)). We reserve this for a future work.

7 COMPARISON WITH NUMERICAL SIMULATIONS

Given a density distribution, the gravitational energy spectrum is uniquely defined. The major uncertainties in our results come from the reconstruction of the 3D density structure.

To access the uncertainty of such a reconstruction, we use simulations from Federrath et al. (2010). The simulations are carried out under pure turbulent initial conditions, and no self-gravity is included. We have chosen this simulation, because (a) turbulence seems to be important in molecular clouds (e.g. Kritsuk et al. 2007; Padoan & Nordlund 2011; Krumholz & McKee 2005; Moeckel & Burkert 2015), and many numerical simulations of star formation are based on initial conditions that are generated from a turbulent box. It would be of theoretical interest to look into the gravitational

energy spectrum from such a turbulent medium, and (b) the simulations seems to exhibit a similar level of complexity to what is actually observed. [3]

The simulations of Federrath et al. (2010) are available at http://starformat.obspm.fr/starformat/project/TURB_BOX. We used the simulation with compressible forcing. The Mach number is $M = 5.6$. The snapshot was taken at $t = 5T$. The simulation is rescaled to a mean H_2 density of 10^3, a sound speed of 0.5 km/s, and a size of 10 pc. A clump of $\sim$ 1 pc in size was separated from the simulation box.

We compute the gravitational energy spectrum of the density structures in this turbulent flow, the results are presented in Fig. 6. The gravitational energy spectrum of the simulation can be described by $E \sim k^{-2.57}$, steeper than what is seen in our observations, but a similar to that of the California molecular cloud (Li & Burkert 2016). For clouds like California, turbulence can provide support against gravity. But for clouds like those seen in the Orion complex, the cloud structure differs significantly from the structures seen in a typical turbulent box, suggesting that gravity is playing a role that is more important that the California.

We compare the gravitational energy spectrum computed directly from the simulation with the spectrum computed based on 3D reconstructions of the 2D projected density distributions. We assume that the observations can reliably trace the density distributions, and the effect of the distribution of dust temperatures, the distribution of gas-to-dust ratios and radiative transfer effects are not modelled. This allows us to access the effect of density reconstruction on the gravitational energy spectrum. The results from the simulation and from the simulated observation exhibit a high degree of resemblance. The gravitational energy spectrum extracted from the simulation is $E \sim k^{-2.57}$, and the result from the simulated observation is $E \sim k^{-2.43}$.

To test the performance of our method under a regime where gravity dominates, we use the simulation from Moeckel & Burkert (2015). The simulation includes self-gravity, and we take a snapshot at 2 times the crossing time when gravity dominates on small scales. We take a subregions of a size of $\sim$ 1 pc, and compare the gravitational energy spectrum derived directly from the simulations with the one reconstructed from the simulation observation. The results are presented in Fig. 7. The gravitational energy spectrum of this gravity-dominated simulation is $E \sim k^{-1.33}$, which is shallower than the energy spectrum of the Burgers turbulence. From the analysis of gravitational energy spectrum alone, one would be able to conclude that gravity is dominating the evolution of the system provided that the system is viralised on the large scale. In both the turbulence-dominated case and the gravity-dominated case, our method performs to an accuracy of 5 %, and is able to constrain the variations of the gravitational energy spectrum to a good accuracy.

The reason for this accuracy of the reconstruction should be discussed briefly. Kainulainen, Federrath & Henning (2014) made a thorough study of the accuracy of density reconstruction on the resulting volume density PDF. Although here we are mainly concerned with the impacts of density reconstruction on the resulting gravitational energy spectrum. Since the major difficulty for both cases is the line-of-sight confusion, how the reconstruction depends on the underlying parameters (e.g. the Mach number and the mode of forcing) should be similar. Kainulainen, Federrath & Henning (2014) found that the density reconstruction performs better for close-to-solenoidal forcing. In this work, to test the robustness of our density reconstruction, we use a simulation with fully compressible forcing. It is also believed that (Federrath et al. 2008) the interstellar medium is dominated by compressible rather than solenoidal modes, consistent with our choice. According to our result, the density reconstruction allows one to evaluate the gravitational energy spectrum to an accuracy of 5 %. This should be taken as a fiducial value, and might change with the complexity of the underlying density structures.

[3] The simulation we have chosen is from a turbulent box without self-gravity. However, as has been demonstrated in Beaumont et al. (2013), gravity acts to modestly reduce the line-of-sight confusion. Thus, the simulation is suitable for testing our method.

Cloud Name	γ_{E_p} analytical	γ_{E_p} this work
Orion A	1.89	1.88
Orion B	2.0	2.17

Table 1. Scaling exponents γ_{E_p} of the gravitational energy spectra for clouds in the Orion complex ($E_p(k) \sim k^{-\gamma_{E_p}}$). "$\gamma_{E_p}$ analytical" stands for the γ_{E_p} inferred from the surface density PDF, using the analytical formulation derived in Li & Burkert (2016), and "γ_{E_p} this work" shows the scaling exponent of the gravitational energy spectra derived from the observations.

The 5 % accuracy of the estimated gravitational energy spectrum can be understood analytically. Suppose that we are measuring the gravitational energy spectrum of a region from 1 pc to 0.1 pc. In our improved density reconstruction method, filamentary structures are preserved. The aspect ratios can be slightly underestimated, but this should not contribute much to the error. This is because gravitational energy is not sensitive to the aspect ratio. An aspect ratio of 10 only changes the gravitational energy estimate by a factor of 1.4. (Bertoldi & McKee 1992; Li & Burkert 2016). For an individual structure, at most, our gravitational energy spectrum can deviate from the real one by a factor of $\log(1.4)/\log(10) \sim 15\%$. This provides a safe estimate of the uncertainties of the estimated slopes of the gravitational energy spectra. This is merely an upper limit. Thus, we expect our method to be more accurate than this. For a typical molecular cloud, there exists a large number of such sub-regions. Assuming these regions are randomly oriented, the error of the estimate should decrease with increasing number N of the regions as $\sim 1/\sqrt{N}$. It is thus understandable that a $\sim 5\%$ accuracy has been achieved.

Another observational constraint should be discussed: In our Orion data, after generating the size map, a diffuse background with a column density of $\sim$ 0.008 $\mathrm{g\,cm^{-2}}$ is not taken into account in the density reconstruction process. This background results from a diffuse component that is larger than e.g. half the box size. It is difficult to tell observationally if this background emission is from the cloud, or whether it is a contribution from foreground/background structures. Nevertheless, because we have limited ourselves to scales that are smaller than half of the box size, our results are not sensitive to this.

s

8 COMPARISON WITH OTHER METHODS

Previously, methods have been proposed to evaluate the impacts of gravity on cloud evolution. Methods such as the virial parameter allows direct comparisons between gravitational energy and e.g. energy from turbulent motion. These methods only allow one to quantify gravity on a given scale, but not across different scales. Because of the complexity of the star formation process, to fully understand

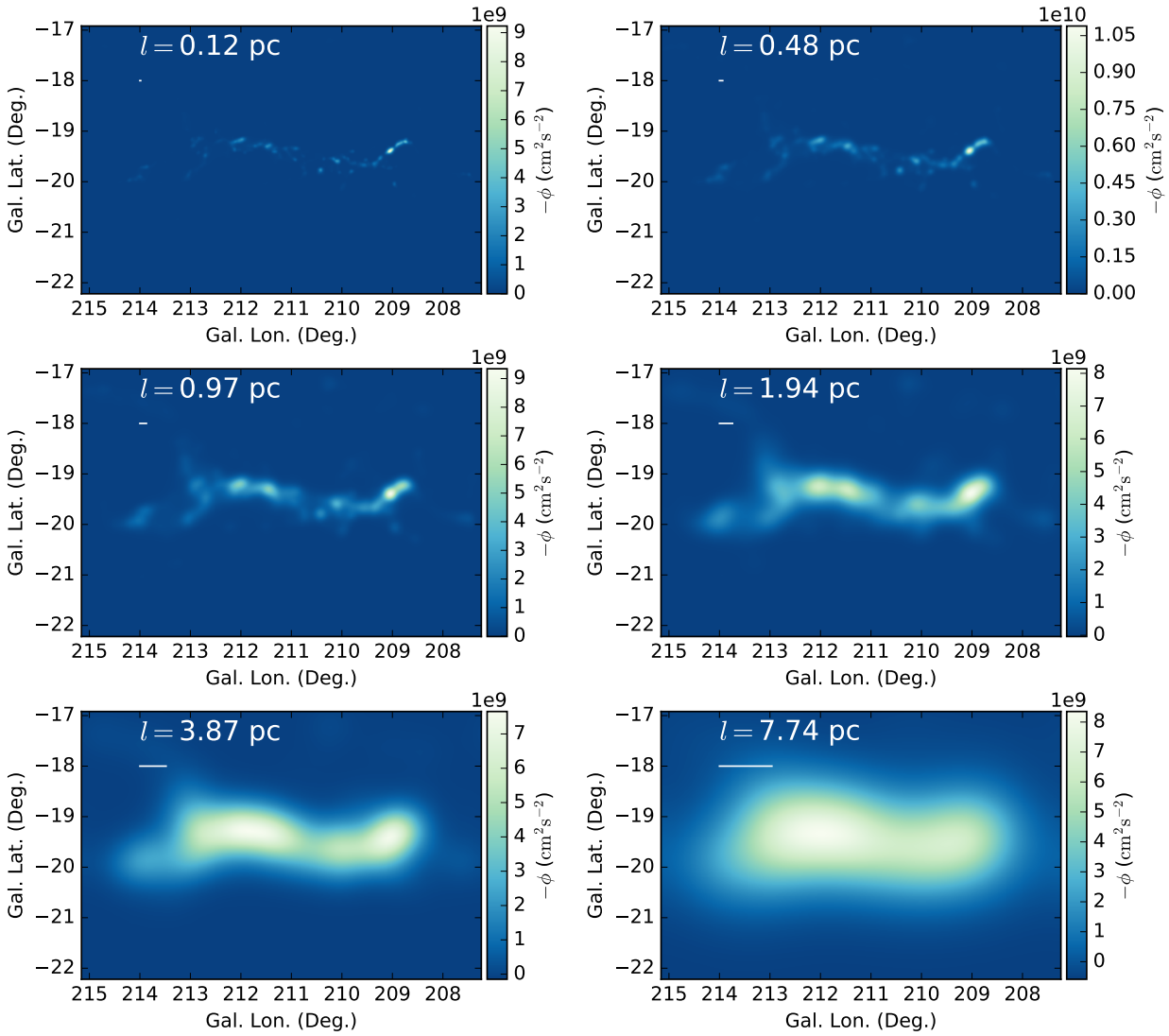

Figure 3. Visualisation of several wavelet components ϕ_l of the gravitational potential of the Orion A molecular cloud, where l is defined in Eq. 2, i.e. the sequence $l = 0.12$ pc, $l = 0.48$ pc, ..., $l = 7.74$ pc correspond to the rough scale of the corresponding wavelet components. Scalebars that indicate the relevant scales are added to the panels. The wavelet components of the gravitational potential are defined in 3D space. The images shown here are produced by taking the minimum of the gravitational potential $\phi(x, y, z)$ along each line of sight. In each panel, l indicate the relevant physical scale of the corresponding wavelet component. When l is small the component is highly structured, and when l is large the component is smoother. Here, one degree correspond to 7.5 pc. The size of the region is ~ 50 pc.

cloud evolution one needs multi-scale methods. Among these, the most commonly-used one is the correlation function. In numerical simulations, it has been demonstrated that the density correlation function can be used to probe the gravitational collapse of molecular clouds (Federrath & Klessen 2013; Burkhart et al. 2015; Collins et al. 2012). Because of gravity, the power spectrum of density can be very shallow and even positive-valued in numerical simulations. This has been suggested by the authors as a clear signature of gravitational collapse.

Indeed, the effect of gravity in cloud evolution can be observed both as variations in the gravitational energy spectrum and as variations in the density power spectrum. Both methods have their own advantages. Here, we emphasise what can be achieved additionally with the gravitational energy spectrum: First, the density power spectrum is a statistical measure, and for the results to be meaningful, it is assumed that the statistics must be close to Gaussian (or log-normal), and the background is approximately statistically homogeneous [4]. Our method is not statistical. It is based on the wavelet transform, and the energies are evaluated through integration over space (Eq. 3). In the cases where the cloud is sig-

[4] These limitations are sometimes mentioned in the literature. One can see e.g. Lazarian & Pogosyan (2016) where the authors propose to combine complementary statistical measures. The gravitational energy spectrum and the density power spectrum does compliment each other in this sense.

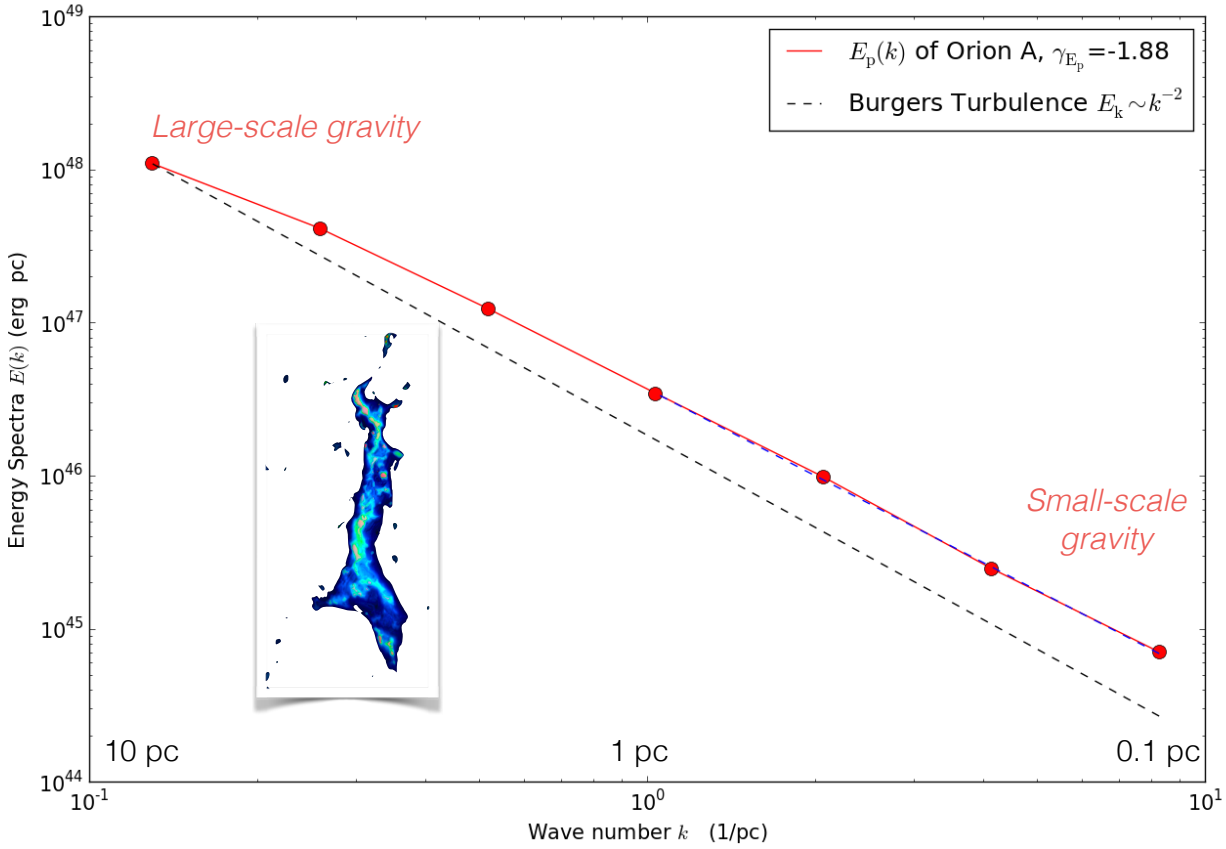

Figure 4. Gravitational energy spectrum of the Orion A molecular cloud. The energy spectrum is shown by the red line. The red cycles show directly the measurements. The x-axis is the wave number $k = 2\pi/l$, l is the length scale, and the y-axis is the energy spectra. $E_{\rm p}(k) \sim k^{-1.88}$ (dashed curve, superimposed on the red curve) provides a fairly good approximation of the gravitational energy spectrum below the parsec scale. This is indicated as the blue dashed line. The black dashed line is the velocity power spectrum of Burgers turbulence. A volume rending of the density structure of the Orion A molecular cloud is included as an inset plot.

nificantly inhomogeneous (e.g. for filaments like the Musca molecular cloud), one can still apply the gravitational energy spectrum to study the scale-dependence of the gravitational energy, but should not apply the density power spectrum blindly. Correlation measures such as the power spectrum are also blind to the phase correlations of the independent Fourier modes (Coles et al. 2004). Second, the gravitational energy spectrum is a measure of gravitational energy as a function of scale. The method is proposed with the intention of comparing various energy terms in molecular clouds (e.g. turbulence, gravitational and magnetic, and perhaps thermal energy), and it measures the amount of gravitational energy as a function of scale. Combined with complimentary measures of velocity structures, we will be able to constrain the interplay between turbulence and gravity to a better accuracy.

One should also note that, obviously, the gravitational energy spectrum and the density power spectrum are different measures, and regions that have the same density power spectrum can have different gravitational energy spectra, and vise versa. A proper combination of these two will provide a better description of the structure of the ISM. This should be explored in the future.

Methods that constrain gravity by synthesising the position and the velocity information include the Dendrogram method and the G-virial method. The Dendrogram method (Rosolowsky et al. 2008) is a generic tool to describe structures seen in observations. Goodman et al. (2009) applied the method to molecular line mapping observations in the PPV (positions-position-velocity) space to constrain gravity on multiple scales, and found that gravity is universally important. The G-virial (Li et al. 2015) method provides constraints on gravity by generalising the concept of gravitational potential to 3D PPV space. The authors compute the virial parameter of the clouds based on the G-virial maps from $\sim$ 0.1 pc to a parsec. They found that the clouds are gravitational bound on multiple scales. It is interesting to note that a similar conclusion has been reached with two almost independent methods. Compared to them, the gravitational energy spectrum offers a different perspective, as it provides constraints of gravity in terms of energy. This would allow one to compare it with turbulence energy and magnetic energy provided that similar constraints are available.

Recently, Li et al. (2016) proposed an acceleration mapping method to constraint the effect of gravity in accelerating gas. The method computes the acceleration induced by large-scale gravity using observational data. They found that acceleration tends to be concentrated in localised regions – as pointed out in Burkert & Hartmann (2004); Hartmann & Burkert (2007). At the cur-

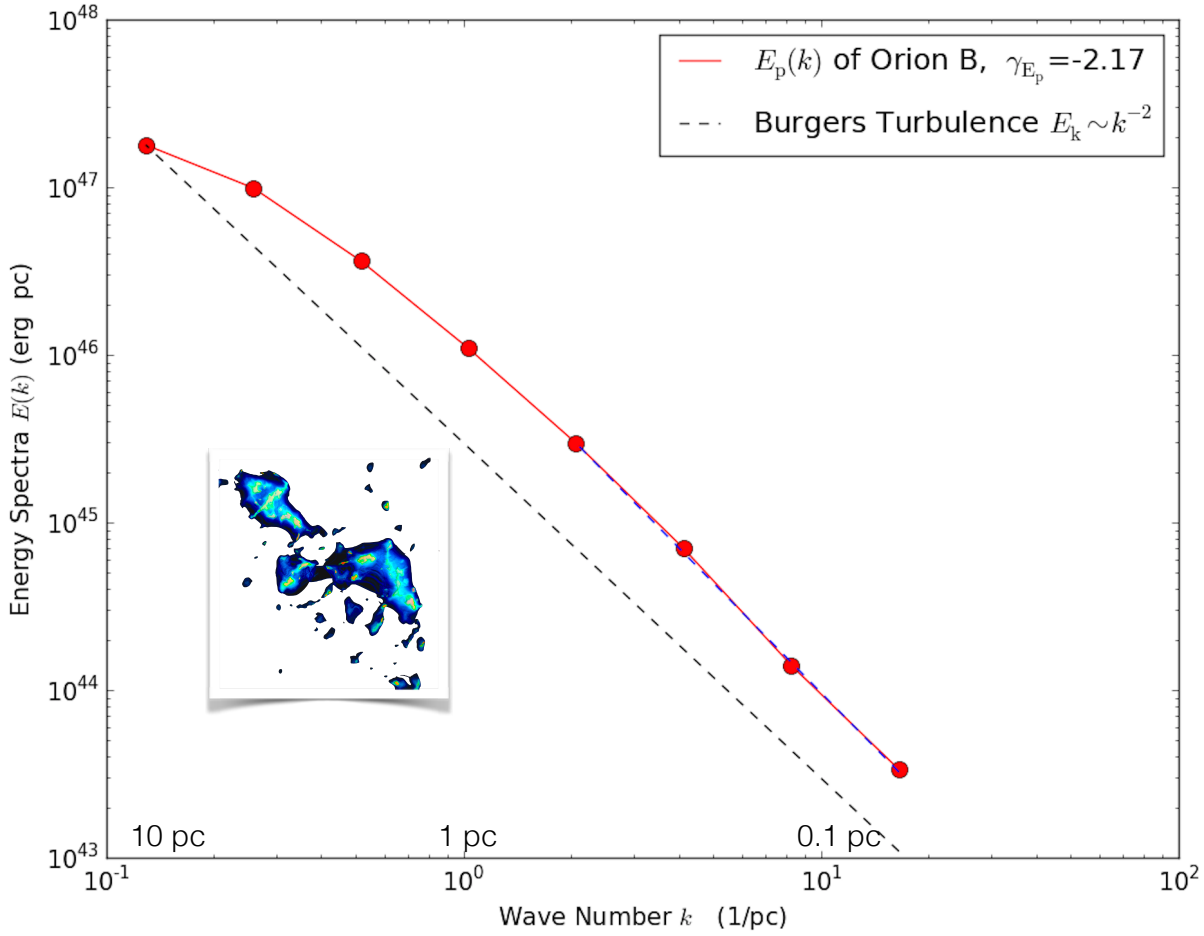

Figure 5. Gravitational energy spectrum of the Orion B molecular cloud. The energy spectrum is shown by the red line. The red cycles show directly the measurements. The x-axis is the wave number $k = 2\pi/l$, l is the length scale, and the y-axis is the energy spectra. $E_{\rm p}(k) \sim k^{-2.17}$ (dashed curve, superimposed on the red curve) provides a fairly good approximation of the gravitational energy spectrum below the parsec scale. This is indicated as the blue dashed line. The black dashed line is the velocity power spectrum of Burgers turbulence. A volume rending of the density structure of the Orion B molecular cloud is included as an inset plot.

rent stage, this method does not provide constraints on gravity in a multi-scaled fashion.

9 CONCLUSIONS

Gravity plays an important role in the evolution of the molecular ISM. In a previous work (Li & Burkert 2016), we proposed a measure called gravitational energy spectrum to quantify the importance of gravity on multiple physical scales. In this work, using a wavelet-based decomposition technique, we derive gravitational energy spectrum of the Orion A and the Orion B molecular cloud. The derived energy spectra cover the range from 0.1 pc to 10 pc, and provide constraints on the importance of gravity on these scales.

It is found that gravitational energy spectra have power law-like shapes. At sub-parsec scale, the Orion A molecular cloud has $E_{\rm p}(k) \sim k^{-1.88}$ and Orion B has $E_{\rm p}(k) \sim k^{-2.09}$. These scaling exponents agree with our earlier analytical estimates (Li & Burkert 2016) to an accuracy of 10 %. The fact that these scaling exponents are close to the exponents of the kinetic energy power spectra of turbulence (where $E_{\rm p} \sim k^{-2}$) indicates a multi-scale equi-partition between turbulence and gravitational energy. It also provides a clear evidence that gravity is able to counteract effectively against turbulence from the cloud scale down to $\sim$ 0.1 pc. For the Orion A molecular cloud, if the cloud as a whole is close to being gravitationally bound, gravity inevitably dominates over turbulence inside the cloud. We also computed the gravitational energy spectrum from the density structure generated from a simulation with a Mach 5.6 compressible turbulence, and found $E_{\rm p} \sim k^{-2.43}$, which is significantly steeper than clouds in the Orion complex but is comparable to e.g. the California molecular cloud (Li & Burkert 2016).

Our work provides a multi-scaled view of molecular cloud dynamics. It demonstrates that turbulent and gravitational energy reaches a rough equi-partition, and proves that gravity is playing an important role in the evolution of turbulent star-forming molecular clouds form the cloud scale down to $\sim$ 0.1 pc. This demands a better understanding of the interplay between turbulence and gravity (perhaps along the path of Vazquez-Semadeni & Gazol (1995); Bonazzola et al. (1987)). Perhaps the dynamics of star-forming molecular clouds could better be described by the hierarchical gravitational collapse model (Hoyle 1953; Elmegreen 1993; Vázquez-Semadeni et al. 2003; Burkert & Hartmann 2013, 2004). Applica-

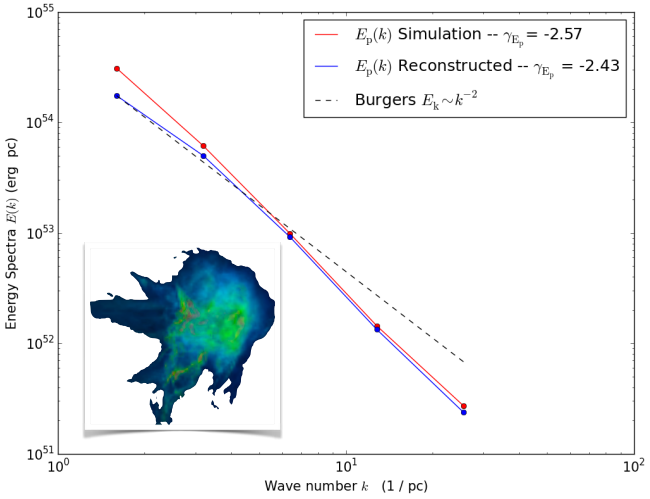

Figure 6. A comparison of the gravitational energy spectrum computed from a Mach 5.6 compressible turbulence from Federrath et al. (2010) and the gravitational energy spectrum reconstructed from the simulated observations. Scaling exponents for both cases are obtained by fitting straight lines in the log-log space. The density structure generated in the simulations have $E_p \sim k^{-2.57}$ and the density structure generated from the simulated observations we obtain $E_p \sim k^{-2.43}$. The black dashed line is the kinetic energy power spectrum of Burgers turbulence. A volume rending of the simulation data is included as an inset plot for reference.

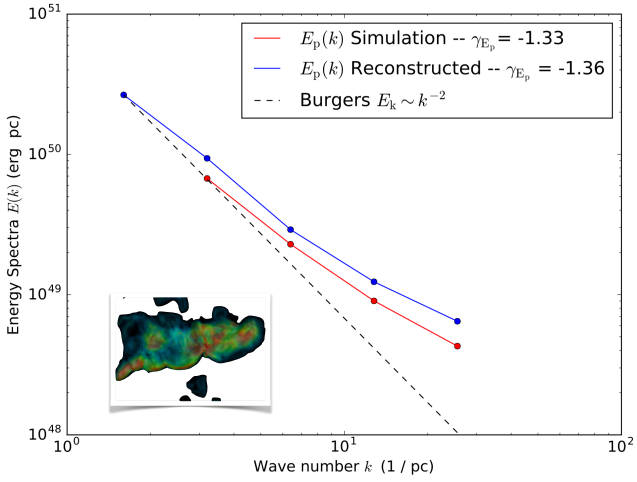

Figure 7. A comparison of the gravitational energy spectrum computed from a $\sim$ 1pc large region obtained from Moeckel & Burkert (2015) and the energy spectrum reconstructed from the simulated observations. Scaling exponents for both cases are obtained by fitting straight lines in the log-log space. The density structure generated in the simulations have $E_p \sim k^{-1.33}$ and the density structure generated from the simulated observations is $E_p \sim k^{-1.36}$. The black dashed line is the kinetic energy power spectrum of Burgers turbulence. A volume rending of the simulation data is included as an inset plot for reference.

tion of the technique to different numerical simulations will help to clarify this issue, and are planned as our future work.

We note, however, that in general molecular clouds have diverse structures. Seen from the perspective of the gravitational energy spectrum, for clouds like Orion A and Orion B (named g-type in Li & Burkert (2016)), gravity is important, for non-star-forming clouds like the California molecular cloud (named t-type in Li & Burkert (2016)), turbulence can dominate.

ACKNOWLEDGEMENTS

Guang-Xing Li is supported by the Deutsche Forschungsgemeinschaft (DFG) priority program 1573 ISM- SPP. The paper also benefits from a careful review from the referee.

APPENDIX A: MULTI-SCALE DECOMPOSITION OF THE SURFACE DENSITY MAP

Kainulainen, Federrath & Henning (2014) proposed to decompose the surface density maps into contributions from structures on different physical scales using the *a trous* wavelet transform, in order to construct the so-called size map. This can be implemented as a series of convolution and subtraction operations. For casual purposes, this approach can provide reasonable results. However, based on filtering in the Fourier space, wavelet transforms are known to produce negative artefacts when the input data is not sufficiently smooth and regular. We first tried to decompose the Herschel-Planck surface density map of Orion A, and found that these negative artefacts contain a significant fraction ($\sim$ 20 %) of the total mass. The articacts are particular pronounced around structures where the column densities are significantly enhanced (e.g. around the cores). We thus developed a new iterative algorithm to decompose the emission map into contributions from structures on different physical scales.

We describe its implementation briefly. The method works by recursively removes significant structures at different resolutions. For each map, the resolution of interest starts from the pixel size to about half of the map size. The coarser resolution is always twice the finer resolution. The procedure starts with the finest resolution.

For a given resolution level $l = 2^k$ ($k = 0, 1, 2, , \ldots$), the emission map $I(x, y)$ is smoothed with a Gaussian kernel whose size (measured in σ) is 2 times of the current resolution, yielding $I_{\rm sm}(x, y)$. Then significant structures are identified as those where $(I(x, y) - I_{\rm sm}(x, y))/I_{\rm sm}(x, y)$ is larger than a given threshold. We experimented with different thresholds, and found that a threshold of 2 gives reasonable results. A change of the threshold does not change the results significantly. These significant structures are stored as a separate array ($I_l(x, y)$, where l represents the current resolution), and are subtracted from the map $I(x, y)$. *This process is repeated until all significant structures have been removed from* $I(x, y)$ *and stored in the array* $I_l(x, y)$. Afterwards, the subtracted emission map contains structures that are $\gtrsim 2$ times the current resolution level. This residual map is smoothed with a Gaussian kernel to ensure that it is sufficiently smooth at the next resolution level, and is passed to the next level of resolution where $l = 2^{k+1}$.

In Fig. A1 we present the size map of the Orion A molecular cloud produced with our recursive algorithm. Different from the wavelet-based decomposition theme, the new iterative algorithm does not produce any negative artefacts.

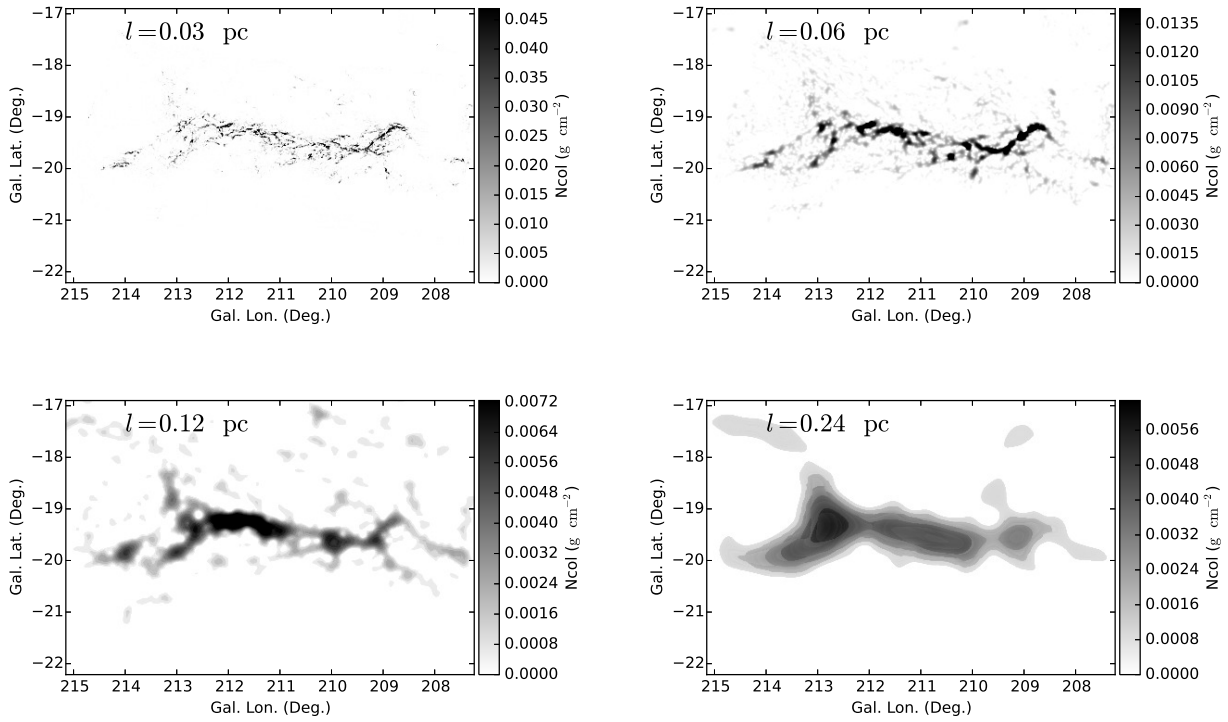

Figure A1. A few channels of the size map of the Orion A molecular cloud. Different maps contain structures of different physical sizes. The relevant physical scales are indicated in the panels. Here l is the dispersion of the Gaussian kernel used for computing the size map. See Sec. A for details.

APPENDIX B: CONTOUR-BASED VOLUME MODELLING

In Kainulainen, Federrath & Henning (2014), the volume density modelling consists of two steps: the first step is to decompose the map into different structures, and the second step is to related the identified 2D structures into 3D structrues.

After decomposing the input density map into contributions from different sizes, the clumpfind algorithm were used to originally identify structures that are later used in reconstructing a 3D density distributions (this step was originally named as "volume density modelling" by these authors). However, in their original formalism, the structures are identified by the clumpfind algorithm (Williams et al. 1994), and were treated as ellipsoids. This introduced sharp edges to the resulting 3D volume density map. The structures identified by "Clumpfind" algorithm blindly should also be considered to be correct only in a statistical sense (Pineda et al. 2009).

For each surface density map $I_l(x, y)$ representing emission contributed from structures of sizes $\sim l$, our method contour-decompose starts from maximum surface density threshold, identifies the significant structures above this threshold, registers them in a catalogue, removes these structures from the emission, and then further decreases the threshold to include less significant structures. This continues until a minimum level is reached. In our calculations, the minimum level above which structures are considered to be significant is set to be 5 % of the maximum level, and for each map we choose 50 equally spaced contour levels.

To put it simple, in our decomposition, the region is split based on a set of contours where the gas inside each contour is taken as an independent structure. Our contour-decompose maximises the use of information in the observed map, and allows one to reconstruct a 3D density map while preserving many of the filamentary structures that also obvious in 2D.

For each of the identified structure, its extent along the line of sight is estimated by diagonalizing the tensors of the second moments of the pixel positions. A 3D density distribution is reconstructed from all the identified structures from our contour-decompose method. The mass distributions along the z direction are modelled by assuming that they follow Gaussian profiles where the dispersion σ is equal to the estimated extent along the third dimension.

For regions like the Orion A, around 10^4 structures are identified and folded into 3D to reconstruct the volume density map. The reconstructed volume density map is in general very smooth.

REFERENCES

Ballesteros-Paredes J., 2006, MNRAS, 372, 443
Bally J., 2008, Overview of the Orion Complex. p. 459
Beaumont C. N., Offner S. S. R., Shetty R., Glover S. C. O., Goodman A. A., 2013, ApJ, 777, 173
Bertoldi F., McKee C. F., 1992, ApJ, 395, 140
Bonazzola S., Heyvaerts J., Falgarone E., Perault M., Puget J. L., 1987, A&A, 172, 293
Burkert A., Hartmann L., 2004, ApJ, 616, 288

Burkert A., Hartmann L., 2013, ApJ, 773, 48
Burkhart B., Collins D. C., Lazarian A., 2015, ApJ, 808, 48
Coles P., Dineen P., Earl J., Wright D., 2004, MNRAS, 350, 989
Collins D. C., Kritsuk A. G., Padoan P., Li H., Xu H., Ustyugov S. D., Norman M. L., 2012, ApJ, 750, 13
Dobbs C. L., et al., 2014, Protostars and Planets VI, pp 3–26
Elmegreen B. G., 1993, ApJ, 419, L29
Federrath C., Klessen R. S., 2013, ApJ, 763, 51
Federrath C., Klessen R. S., Schmidt W., 2008, ApJ, 688, L79
Federrath C., Roman-Duval J., Klessen R. S., Schmidt W., Mac Low M.-M., 2010, A&A, 512, A81
Goldsmith P. F., Heyer M., Narayanan G., Snell R., Li D., Brunt C., 2008, ApJ, 680, 428
Goodman A. A., Rosolowsky E. W., Borkin M. A., Foster J. B., Halle M., Kauffmann J., Pineda J. E., 2009, Nature, 457, 63
Hartmann L., Burkert A., 2007, ApJ, 654, 988
Heyer M., Krawczyk C., Duval J., Jackson J. M., 2009, ApJ, 699, 1092
Hoyle F., 1953, ApJ, 118, 513
Ibáñez-Mejía J. C., Mac Low M.-M., Klessen R. S., Baczynski C., 2015, preprint, (arXiv:1511.05602)
Kainulainen J., Federrath C., Henning T., 2014, Science, 344, 183
Klessen R. S., Hennebelle P., 2010, A&A, 520, A17
Kritsuk A. G., Norman M. L., 2011, preprint, (arXiv:1111.2827)
Kritsuk A. G., Norman M. L., Padoan P., Wagner R., 2007, ApJ, 665, 416
Krumholz M. R., McKee C. F., 2005, ApJ, 630, 250
Lazarian A., Pogosyan D., 2016, ApJ, 818, 178
Li G.-X., Burkert A., 2016, MNRAS, 461, 3027
Li H.-B., Goodman A., Sridharan T. K., Houde M., Li Z.-Y., Novak G., Tang K. S., 2014, Protostars and Planets VI, pp 101–123
Li G.-X., Wyrowski F., Menten K., Megeath T., Shi X., 2015, A&A, 578, A97
Li G.-X., Burkert A., Megeath T., Wyrowski F., 2016, preprint, (arXiv:1603.05720)
Lombardi M., Bouy H., Alves J., Lada C. J., 2014, A&A, 566, A45
Lombardi M., Alves J., Lada C. J., 2015, A&A, 576, L1
Mac Low M.-M., Klessen R. S., 2004, Reviews of Modern Physics, 76, 125
Men'shchikov A., et al., 2010, A&A, 518, L103
Menten K. M., Reid M. J., Forbrich J., Brunthaler A., 2007, A&A, 474, 515
Moeckel N., Burkert A., 2015, ApJ, 807, 67
Padoan P., Nordlund Å., 2011, ApJ, 730, 40
Pineda J. E., Rosolowsky E. W., Goodman A. A., 2009, ApJ, 699, L134
Roman-Duval J., Jackson J. M., Heyer M., Rathborne J., Simon R., 2010, ApJ, 723, 492
Rosolowsky E. W., Pineda J. E., Kauffmann J., Goodman A. A., 2008, ApJ, 679, 1338
Schneider S., Elmegreen B. G., 1979, ApJS, 41, 87
Starck J.-L., Murtagh F. D., Bijaoui A., 1998, Image Processing and Data Analysis
Stutz A. M., Kainulainen J., 2015, A&A, 577, L6
Traficante A., Fuller G. A., Smith R., Billot N., Duarte-Cabral A., Peretto N., Molinari S., Pineda J. E., 2015, preprint, (arXiv:1511.03670)
Vazquez-Semadeni E., Gazol A., 1995, A&A, 303, 204
Vázquez-Semadeni E., Ballesteros-Paredes J., Klessen R. S., 2003, ApJ, 585, L131
Wienen M., Wyrowski F., Schuller F., Menten K. M., Walmsley C. M., Bronfman L., Motte F., 2012, A&A, 544, A146
Williams J. P., de Geus E. J., Blitz L., 1994, ApJ, 428, 693
Williams J. P., Blitz L., McKee C. F., 2000, Protostars and Planets IV, p. 97